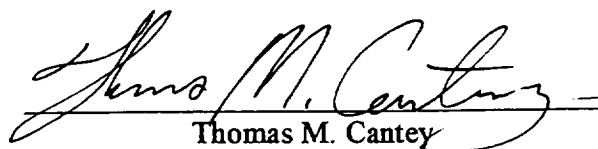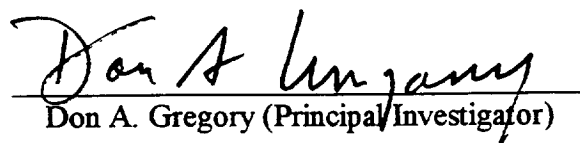FINAL

IN -74 -CK

O CIT

OC3 78

FINAL REPORT

ION FIGURING OF X-RAY MIRROR MANDRELS

Period of Performance:
June 14, 1996 to June 5,1997

Contract No. NAS83-8609 D.O. 166

Thomas M. Cantey

Don A. Gregory (Principal Investigator)

Completed under:

UAH DELIVERY ORDER 166

JUNE 1997

Submitted to:

NASA/MSFC

Submitted by:

University of Alabama in Huntsville
Department of Physics
Huntsville, AL 35899

REPORT DOCUMENTATION PAGE

Form Approved
OMB No. 0704-0188

1a. REPORT SECURITY CLASSIFICATION	1b. RESTRICTIVE MARKINGS
2a. SECURITY CLASSIFICATION AUTHORITY	3. DISTRIBUTION/AVAILABILITY OF REPORT
2b. DECLASSIFICATION/DOWNGRADING SCHEDULE	

4. PERFORMING ORGANIZATION REPORT NUMBER(S)	5. MONITORING ORGANIZATION REPORT NUMBER(S)

6a. NAME OF PERFORMING ORGANIZATION	6b. OFFICE SYMBOL (If applicable)	7a. NAME OF MONITORING ORGANIZATION
University of Alabama in Huntsville		

6c. ADDRESS (City, State, and ZIP Code)	7b. ADDRESS (City, State, and ZIP Code)
Huntsville, AL 35899	

8a. NAME OF FUNDING/SPONSORING ORGANIZATION	8b. OFFICE SYMBOL (If applicable)	9. PROCUREMENT INSTRUMENT IDENTIFICATION NUMBER
NASA		

8c. ADDRESS (City, State, and ZIP Code)	10. SOURCE OF FUNDING NUMBERS			
Washington, D.C. 20546-0001 Marshall Space Flight Center, AL 35812	PROGRAM ELEMENT NO.	PROJECT NO.	TASK NO.	WORK UNIT ACCESSION NO.

11. TITLE (Include Security Classification)

Ion Beam Figuring of Replicated X-ray Optics

12. PERSONAL AUTHOR(S)

Thomas M. Cantey, Don A. Gregory

13a. TYPE OF REPORT	13b. TIME COVERED	14. DATE OF REPORT (Year, Month, Day)	15. PAGE COUNT
Final	FROM 5/96 TO 6/97	1997, June 30	50

16. SUPPLEMENTARY NOTATION

17. COSATI CODES			18. SUBJECT TERMS (Continue on reverse if necessary and identify by block number)
FIELD	GROUP	SUB-GROUP	

19. ABSTRACT (Continue on reverse if necessary and identify by block number)

This investigation included experiments to demonstrate ion beam figuring effects on electrole
nickel with the expressed desire to final figure X-ray optic mandrels. It was important to
establish that ion beam figuring did not induce any adverse effects to the nickel surface.
The ion beam has consistently been shown to be an excellent indicator of the quality of the
subsurface. Polishing is not the only cause for failure in the ion beam final figuring proce
the material composition is equally important. Only by careful consideration of both these
factors can the ion beam final figuring process achieve its greatest potential.

The secondary goal was to construct a model for representing the ion beam material removal ra
Representing the ion beam removal rate is only an approximation and has a number of limiting
factors. The method developed for determining the beam function has broad application to any
material destined to be ion beam figured.

20. DISTRIBUTION/AVAILABILITY OF ABSTRACT	21. ABSTRACT SECURITY CLASSIFICATION
☐ UNCLASSIFIED/UNLIMITED ☐ SAME AS RPT ☐ DTIC USERS	

22a. NAME OF RESPONSIBLE INDIVIDUAL	22b. TELEPHONE (Include Area Code)	22c. OFFICE SYMBOL

DD Form 1473, JUN 86   Previous editions are obsolete

Abstract
Ion Beam Figuring of Replicated X-ray Optics

This investigation included experiments to demonstrate ion beam figuring effects on electroless nickel. It was important to establish that ion beam figuring did not induce any adverse effects to the nickel surface. When using ion beam figuring for the final figuring it is critical to have a stress free surface and subsurface devoid of defects or damage. The ion beam has consistently been shown to be an excellent indicator of the quality of the subsurface. Polishing is not the only cause for failure in the ion beam final figuring process, the material composition is equally important. For ideal removal of material the material being figured has to be homogeneous. Only by careful consideration of both these limiting factors can the ion beam final figuring process achieve its greatest potential.

The secondary goal was to construct a model for representing the ion beam material removal rate. Representing the ion beam removal rate is only an approximation and has a number of limiting factors. The resolution of the metrology apparatus limits the modeling of the beam function as well. As the surface error corrections demand more precision in the final figuring, the model representing beam function must be equally precise. The precision to which the beam function can be represented is not only determined by the model but also by the measurements producing that model. The method for determining the beam function has broad application to any material destined to be ion beam figured.

Acknowledgments

The research described in this final report were made possible by the fine people at Marshall Space Flight Center and the University of Alabama in Huntsville for giving me the chance to aid them in their scientific endeavor. First I would thank Don A. Gregory for placing his trust in me and bestowing divine guidance. William Jones and James Bilbro deserve great praise for making this research opportunity possible and insuring I had everything I needed.

I would also like to thank the insight and instruction of Tom Kester, the master lapidary Charlie Griffiths and the many talks with Darell Engelhaupt. Lastly, I would like to thank all my friends and family and especially Jennie.

TABLE OF CONTENTS

LIST OF FIGURES

LIST OF TABLES

LIST OF SYMBOLS

Symbol	Definition
$B(x,y)$	Beam function (ion beam removal rate profile).
C	Width of the scanning strip.
Γ	Peak removal rate of the ion beam.
ω	Ion beam width in the Gaussian distribution model.
$R(x,y)$	The "hit" map or removal map.
s	Width of scanning strip in integration of dwell function.
$T(x,y)$	Dwell function.
$V(x,y)$	Scanning velocity of the ion beam.

1. Introduction

Ion beam figuring of large optics has proven to be successful and is currently being used in the fabrication process for optical components. Eastman Kodak figures 2.5 meter optics in its fabrication system[1] and Oak Ridge National laboratory figures 60 cm optics[13]. There has been limited experimentation in figuring smaller optics under 30 cm and the effects on the surface as a result of ion beam figuring. An exception is the previous work by Drueding with near-flat circular optics under 80 mm diameter[14-16]. Ion beam figuring has shown two clear advantages over conventional contact methods of final figuring. The process is more efficient, especially in preventing edge roll off, and does not typically increase the surface roughness of the workpiece. For these reasons there has been a push to develop a Precision Ion Machining System (PIMS) at NASA's Marshall Space Flight Center. The completed project should show an ion beam can impart a contour on plated electroless nickel mandrels used in the replication of X-ray optics without significant degradation of the surface microroughness. Ion beam figuring is a desirable method of final figuring because there is no contact with the workpiece. The non-contact method reduces workpiece stress and prevents warping or deformation. This process relies totally on neutralized particles of the ion beam impinging on the work area to remove material through a transfer of kinetic energy[14].

The ion beam source used in this investigation is a broad beam Kaufman type[20] which produces a plasma formed in a discharge chamber regulated by electric potentials. The ions in the chamber are accelerated using charged electric grids, thus forming the ion beam. The ion beam is charge neutralized after the grids by a current carrying filament[14]. This is a

necessary step to insure the prevention of workpiece charging and minimize distortion and deviation of the beam by electromagnetic fields.

The ion beam profile is defined as the material removal rate which is a function of the distance from the beam center. This is determined for each material to be figured to guarantee accurate final figuring. The beam profile is normally modeled by a Gaussian function[14,15], and experiments by Drueding showed this to be satisfactory, yielding high accuracy for a stable beam. The beam profile is a fixed function for a stable beam and produces a constant removal rate when the beam parameters are held constant. Therefore, the amount of material removed can be determined by the time the beam dwells at a certain location.

The stability of the ion beam is the key to the success of the final figuring process. The ion beam has to be temporally and spatially stable to produce predictable results. This assures a constant removal rate at different distances from the ion beam's center peak intensity. Specific contours can be figured allowing the beam to dwell for different lengths of time to remove the necessary amount of material[14,15]. The ion beam can be allowed to dwell in designated locations for the appropriate times or scanned across the workpiece at specific velocities.

The ion beam final figuring process being developed follows the typical steps of conventional polishing only with fewer iterations and has the potential to be incorporated into a single process. The first step is to determine the initial contour of the workpiece and its deviation from the desired contour. The initial contour is interferometrically mapped by a Zygo Interferometer Mark IV or a Trace Profilometer. This initial contour is then subtracted from the desired contour to get a map of the material to be removed. This is the removal map or

target "hit" map[14,15]. The beam profile will be characterized prior to the material being ion figured. The parameters will be set to insure a constant removal rate, so the dwell time determines the specified amount of material to be removed. The dwell function can be used to determine the velocity of the ion beam sweeping across the workpiece, and depends on the amount of material to be removed. The amount of material to be removed is a convolution of the beam profile function and the dwell function, hence the dwell function may be determined by a deconvolution[14-16]. The results of ion beam figuring hinge on creating a stable beam and an accurate model of the ion beam removal profile.

The Precision Ion Machining System (PIMS) will later be expanded to perform final figuring of cylindrical grazing incidence optics. Specifically, these pieces will be the mandrels for replicating the grazing incident X-ray optics. Previous work developed the PIMS for final figuring of small optical components made of fused silica and chemical-vapor-deposited SiC [14][15]. The mandrels to be ion figured are composed of aluminum plated with electroless nickel. The questions are: can electroless nickel be ion figured without significant degradation of the surface finish or deformation, and how will the ion beam removal profile be affected by the mandrel's cylindrical target?

The first phase of the project was to characterize the ion beam removal rate and beam profile. This was exceptionally difficult, in that the ion beam's width is equivalent to the radius of the mandrel. Therefore, the impinging neutral atoms will have to be characterized by angle of incidence, throughout the beam, on the cylindrical target. The most efficient removal rate will be determined for the ion beam and the parameters for this beam profile will be maintained

for maximum beam stability. Control of the ion beam's profile is the key to the success of the figuring process. It must be deterministic and efficient.

The cylindrical mandrel's surface will be mapped and compared to the ideal mathematical model, thus determining the error regions. Interferometry analysis is one method purposed for mapping the irregularities of the mandrel surface[21,22]. The interferometry technique should be very sensitive in revealing irregularities in the mandrel surface. An alternate mapping method could include a Long Trace Profilometer analysis down the axis of the mandrel. The error regions can be identified and isolated by assuming axial symmetry and comparing to the ideal contour. If axial symmetry is assumed the contour algorithm reduces to a one dimensional problem.

The PIMS will be adapted to show the potential success in correcting surface contours in the final figuring of cylindrical optics. Attempts to focus the ion beam without compromising volumetric removal rate will be continued as was done in initial beam aperture experiments by Drueding[14,15]. The milling of desired contours will be determined by an adaptation from a deconvolution using a series-derivative solution[14,16]. This will insure the predictability of the milling depth, material removed, and the beam sweep velocity across the surface.

The goal will be to demonstrate that ion beam figuring is capable of imparting a desired contour on a mandrel surface. The quality of the X-ray optic will depend on the surface precision and accuracy.

2. Ion Beam Machining History

Ion beam figuring is a fairly recent technology promising higher performance optical finishing techniques. The industry is constantly driven to provide economically and technologically superior processes to meet the demand and needs of the market. Ion beam figuring has shown a great advantage in the final figuring process of large optics, greater than 30 cm. Ion beam figuring is unique in that it relies on the kinetic interaction of ions and atoms (or molecules) on the surface to remove material. The success of ion beam figuring programs is due to the deterministic behavior of the beam removal rate, and the fact ion bombardment does not damage the surface and render it optically useless. The most current example of commercial success in figuring large optics is the ion beam figuring systems employed by Eastman Kodak Company and Oak Ridge National Laboratory. Present research is concentrated on ion beam figuring of small optics, less than 30 cm, and mandrels for replication of X-ray optics. The mandrel figuring is especially interesting because the material's surface is cylindrical and consists of electroless nickel. This is the figuring issue addressed in this thesis.

The exploration of ion beam figuring began in the 1960's in the semiconductor industry[1-5]. Ion beam figuring at that time for optical surfaces was found to be impractical using Cockroft-Walton accelerator sources[6]. These were large ion beam sources driven by very high ion energies producing a beam current in the hundred microampere range. The optical surface was rendered useless at these exceptionally high ion energies because of radiation damage to the target material[7,8].

5

The Kaufman ion source[9] of the late 1970's, promised to be a good candidate for precision surface machining. The ion source characteristics that made this possible were the ion energy ranges of 300-1500 eV, producing high beam currents close to an ampere, acceptable for possible optical figuring. In addition, the ion beam consistently showed great stability and control[6].

Scott Wilson, in 1987 at the University of New Mexico, conducted a series of ion beam experiments in figuring large optical surfaces showing the speed, accuracy, and effectiveness of this method of final figuring[6]. Wilson's use of image processing in modeling the figuring process proved effective and informative[6]. Limitations of this prototype system were due to the metrology accuracy and the deconvolution calculation that limited noise filtering.

The Eastman Kodak Company recently developed an ion figuring system for large optical fabrication that has proven to be an effective and deterministic optical fabrication method[10]. The Ion figuring System (IFS) is a five-axis computer controlled system capable of final figuring of large optics up to 2-3 meters in diameter. IFS modeling results have shown potential for rapidly converging to the required optical surface figures. The Kodak IFS successfully corrected the surface error of a Keck 10 m telescope primary mirror segment in 1991[11]. The IFS also effectively performed the final surface error correction of an off-axis aspheric petal[12].

Oak Ridge National Laboratory also operates an ion beam figuring system. The system utilizes its own Advanced Matrix-Based Algorithm for control of the ion beam milling of optical components. The algorithm was developed in 1992 to reduce the noise sensitivity

and achieve a surface profile close to the desired surface with a trade-off for milling time and allowable piston error[13]. The system can currently figure 60 cm size optical components.

Thomas Drueding, in 1995, performed ion beam figuring of small 80 mm optical components at NASA's Marshall Space Flight Center using the Precision Ion Machining System (PIMS), which he helped develop. Drueding analyzed the effects of ion beam figuring on surface roughness using a 3 cm Kaufman filament type ion source. Results showed that when fabricating ceramic mirrors to achieve greatest optical quality, it was best to employ a deterministic ductile-grinding operation followed then only by a final ion beam figuring process[14,15]. Utilization of the ion beam in this fashion is an excellent indicator of subsurface damage and material imperfections. Another key development was a unique method for performing a deconvolution for determining the dwell function[16]. The dwell function is the time the ion beam will remain in any given area on the workpiece to remove the desired amount of material over that area. The algorithm consequently has applications in computer controlled polishing as well. The experiments successfully demonstrated the operation of the PIMS in figuring small 80 mm fused Silica and CVD SiC samples.

2.1. Theory

Ion beam figuring has advantages and disadvantages compared to mechanical figuring. The significant advantages are the elimination of surface contact with the tool, no edge roll off effect and no weight loaded onto the workpiece. Other benefits are the high removal rates, effective surface correction of centimeter spatial wavelength errors, and the advantages of

figuring and coating on site without moving the workpiece. The deterministic nature of the ion beam removal rate makes it ideal for precision machining.

The drawbacks are the high temperatures introduced to the workpiece, the potential increase in surface roughness, and the vacuum chamber needed to house the operation. The vacuum is reasonably low, 10e-4 torr, so this disadvantage is minor. The material must also be characterized before any machining to determine the manufacturing effects and removal rates.

Conventional methods used to final figure optical components is an iterative process of polishing and metrology. The basic procedure breaks down into several stages. The process begins with the procured optical component, which can be roughly shaped by sawing and grinding. The second stage removes less material by a carefully controlled grinding until the component requires only a small amount of material to be removed to gain the desired figure.

The next stage is the iterative figuring process. Material is removed by pitch polishing, and then the surface is inspected to provide information on required repetition of this step. This is a time consuming process and time drives up the price of an optic. Computer controlled polishing can enhance the iterative process, but does little to affect the cost. Upon completion of this stage the final step is to clean and coat the optic.

Ion beam figuring technology is designed to replace the iterative polishing and metrology stage. The optic can be polished to provide microroughness characteristics and then mapped using established metrology techniques. The polishing to a microroughness state means there are few subwavelength corrections to contend with which the ion beam cannot correct. The metrology provides the ion beam figuring control with a "hit" map of the error regions deviating from the desired contour. The optic is then figured using an ion beam to

remove the aberrations from the surface. The optic can be coated immediately after the figuring process because the ion beam atomically cleans the surface. After an inspection the optic is ready for use.

The ion beam figuring process involves a critical relationship between the ion beam energy profile and how that energy is delivered to the workpiece. There are four key factors which are to be understood in this relationship: (1) the energy of the beam, (2) the material being figured, (3) distance from workpiece and (4) angle of incidence[14,15]. The ion beam is usually at a fixed distance and perpendicular to the workpiece. The ion beam current density is set to insure a constant removal rate. The figuring process scans the ion beam across the workpiece at specific velocities to insure the removal of a specified amount of material.

The material removal process is a convolution of the ion beam removal profile (beam function) and the dwell function, which ideally will equal the "hit" map of the material to be removed. The convolution is a consequence of the ion beam removing material over a broad area[14]. The material must first be characterized before the figuring process can begin. This entails determining the beam function. Only then can the dwell function be calculated by performing a deconvolution between the beam function and the "hit" map.

The beam function, $B(x,y)$, is determined by the intensity of the ion bombardment and the shape this intensity manifests. Both these parameters will be invariant under stable and constant removal rates at any point. Units are depth of material removed per exposure time. The beam function must be determined for each material being figured because different materials respond differently.

The material to be removed is the "hit" map, R(x,y), and is calculated by subtracting the figuring surface contour from the desired surface contour. Thus resulting in a map which can then be targeted by the ion beam figuring system's algorithm. The limitations of the procedure are most clearly realized at this point. The resolution of the figuring process depends heavily on the metrological map of the surface contour and the ability to represent and manipulate that map. Any further improvement to the surface contour would be concealed in the resolution limited region.

The material to be removed is a convolution of the beam function, B(x,y), and the dwell function, T(x,y),

$$R(x,y) = \int_{-\infty}^{\infty} \int_{-\infty}^{\infty} B(x-u, y-v)T(u,v)dudv = B(x,y) * T(x,y) \qquad (1)$$

where the convolution is denoted with an asterisk. The material removed from the workpiece is the removal function, R(x,y) where ideally this would be equal to the "hit" map. The workpiece can now be assigned a scanning strip of width, C where the ion beam will be scanned at particular velocities sufficient to remove the desired material along that strip, determined by the dwell function, T(x,y). The dwell function in turn is determined by the deconvolution of the beam function and "hit" map. The units of the dwell function are time per area, thus the scanning velocity, V(x,y), is the inverse of the dwell function integrated over the scanning strip width, C where s in this case is the width of the strip.

$$V(x,y) = \frac{1}{\int_c T(x,y)ds} \qquad (2)$$

The scanning velocities correspond to particular regions of the workpiece and will be input parameters for the figuring control system.

The optical workpiece can converge to the desired contour quite rapidly in one or more iterations. Thus making the ion beam figuring a less time consuming process than conventional final figuring methods. The advantages are less time to completion of precision optics of superior quality and a more reasonable cost.

3. Ion Figuring Apparatus and Metrology Equipment

The ion figuring system used was a prototype Precision Ion Machining System (PIMS) in development at NASA's Marshall Space Flight Center and first assembled by Steve Fawcett and Thomas Drueding for the purpose of ion figuring small ceramic optics. The PIMS shown in Figure 3.1 consists of a 30 inch vacuum sputtering chamber outfitted with an On-Board cryopump. The ion source is a 3 cm broad beam Kaufman filament type schematically represented in Figure 3.2 and controlled by an MPS-3000 FC Ion Tech, Inc. power supply[23]. The feeder gas for the plasma is argon and is controlled by a mass flow control valve and a Gas Flow Controller (GFC-1000). Both the power supply and the gas flow controller are programmable and interface with a 80486 Personal Computer. The ion source and/or workpiece can be translated by motion control stages in order to scan the workpiece with the ion source in the machining process. The translation stages have two configurations, (1) one for the small circular optics and (2) another for the small cylindrical mandrels.

The surface contour was mapped using a ZYGO Mark IV interferometer for the flat optics, and mapped experimentally using a Long Trace Profilometer LTP II, developed by Continental Optical Corporation, for the cylindrical optics. The surface contours were saved as Zernike polynomials and manipulated using Mathematica. The surface microroughness was measured using a WYKO 3-D Profilometer.
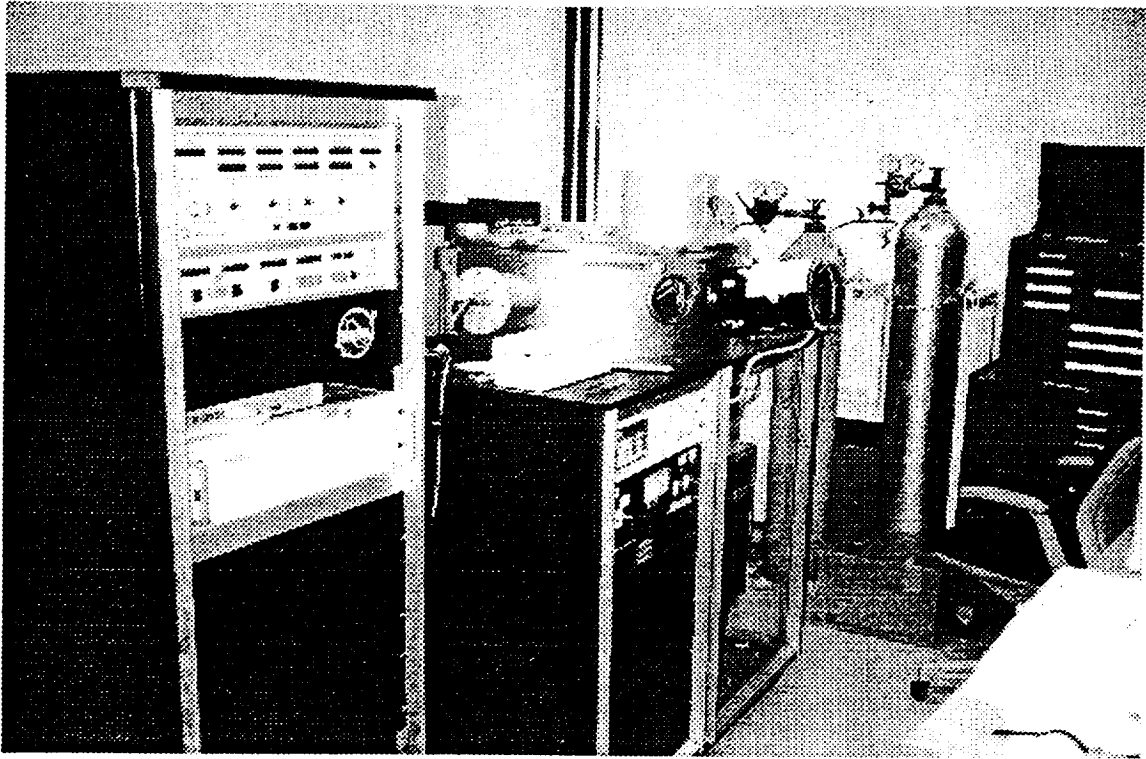
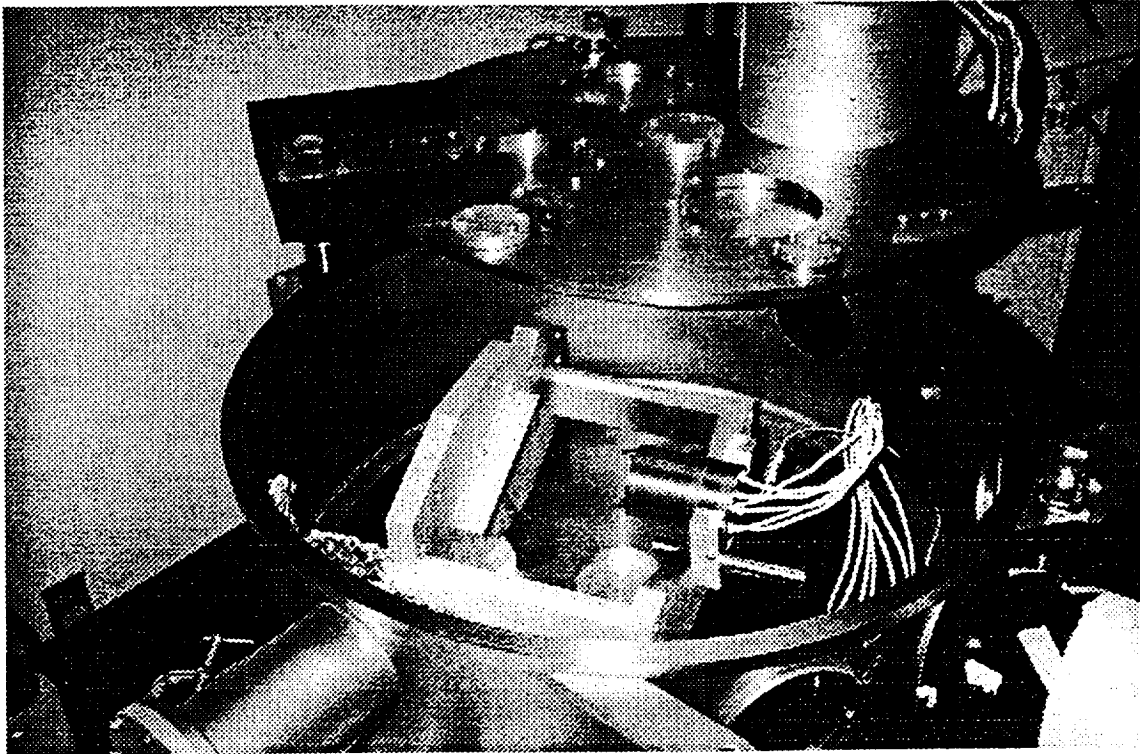Figure 3.1   Precision Ion Machining System (PIMS).

Figure 3.2   Ion Source viewed in vacuum chamber.

4. Ion Beam Operation Parameters

The Kaufman type broad beam 3 cm ion source was provided by Ion Tech, Inc. including a programmable power supply and Gas Flow Controller. The MPS-3000 FC power supply proved to be very reliable and stable. The individual power supplies within the unit allow for each of the ion source parameters to be powered separately, increasing the stability of the ion beam. The Gas Flow Controller maintains the feeder argon gas at a constant rate to insure adequate plasma discharge. The Ion Tech, Inc. system showed to provided excellent stability and flawless reliability.

The ion beam parameters are the current and voltage values input into the power supply to operate the ion source. The objective was to focus the ion beam using these parameters to the achieve the smallest spot size without compromising the removal rate of material. The best parameters were:

	Discharge	Beam	Acceleration
Current	0.88 amps	60 microamps	1 microamps
Voltage	55 volts	1000 volts	200 volts

Table 4.1   Ion beam operation parameters.

The discharge voltage regulates the discharge chamber plasma. The beam current is proportional to the plasma density inside the discharge chamber[23]. A high beam current means an increased removal rate of material. The acceleration current is a measure of the

ions leaving the discharge chamber. The acceleration voltage creates the potential difference to draw the ions from the discharge chamber. When large numbers of ions are accelerated through the acceleration grids the repulsive forces have a tendency to disperse to ion beam before it is neutralized. Having the lowest possible acceleration voltage without the back streaming of electrons from the neutralizing filament creates the narrowest beam.

The parameters in Table 4.1 were used in the following experiments with great success. For greatest removal rate of material and smallest spot size, these are the suggested parameters.

5. Surface Microroughness Experiment on Electroless Nickel

There are two major polishing techniques used to final figure electroless nickel, diamond paste compound and aluminum oxide followed by a silica based colloidal pitch polish. The nickel surface being polished must achieve a microroughness below 5 angstroms to prevent any unnecessary scattering of X-rays when the surface finish is transferred to the replicated optics. High energy X-rays are very sensitive to surface anomalies of an optic and at grazing incidence the sensitivity is a critical factor in reducing scattering. The best polishing process for electroless nickel will provide the lowest microroughness RMS and inflict the least amount of subsurface damage. The ion source was chosen because it is an excellent indicator of subsurface damage as demonstrated by Drueding[14,24]. It is critical to have a clear picture of the effects of exposing electroless nickel to an ion source in a deterministic process as final figuring. The evolution of the surface microroughness must not significantly increase due to the exposure time or the machining depth of the ion beam.

5.1. Diamond vs. Aluminum Oxide Polishing

The experiment was to compare two 2 inch flat circular samples plated in the same bath of electroless nickel, diamond turned to 60 angstroms and polished with either diamond paste compound or aluminum oxide followed by a silica based colloidal pitch polish.

The diamond paste compound was not successful in achieving an RMS below 15 angstroms. Even stepping down the paste grit size did not surpass the 15 angstrom

barrier. Using the ion beam source as an indicator for subsurface damage led to the diamond paste polish as the limiting agent, as opposed to defects introduced in the electroless nickel plating process. When the ion beam was exposed to the nickel surface, the neutral atoms bombarded the surface removing the nickel, but leaving behind sharp spikes. These spikes, sometimes called stickers, were uncovered by the ion beam removing the nickel which suggested the stickers were not composed of the assumed homogeneous electroless nickel. The diamond particles are very hard and have a tendency to become embedded in the nickel creating theses stickers when the otherwise homogeneous nickel around it is removed. The diamond particles can be seen in a micrograph as glistening points in Figure 5.1.

The RMS evolution measured by a WYKO 3-D profilometer in Figure 5.2 also contributes evidence to support diamond particles embedding in the nickel. The RMS immediately rose to 18 angstroms then 22 angstroms after only two 10 second exposures to the ion beam from an initial microroughness of 15 angstroms. The next four minutes the RMS levels remained at 22 angstroms, as if it had exposed all the embedded diamond and was only making the stickers larger and more dominant features. The Peak to Valley ratio in Figure 5.3 follows this argument with a steady increase in its value. Once the diamond is embedded, even if the ion beam does finally remove the particle, the diamond has made its mark on the surface at such a small point that the broad ion beam is unable to correct it.
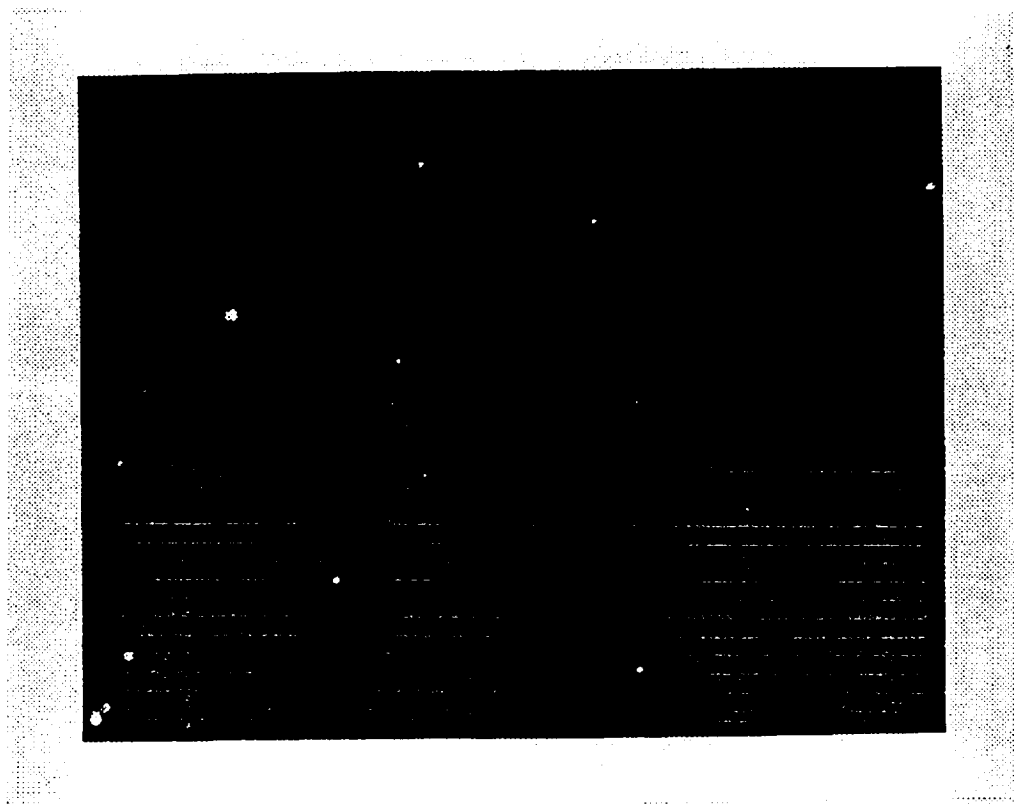
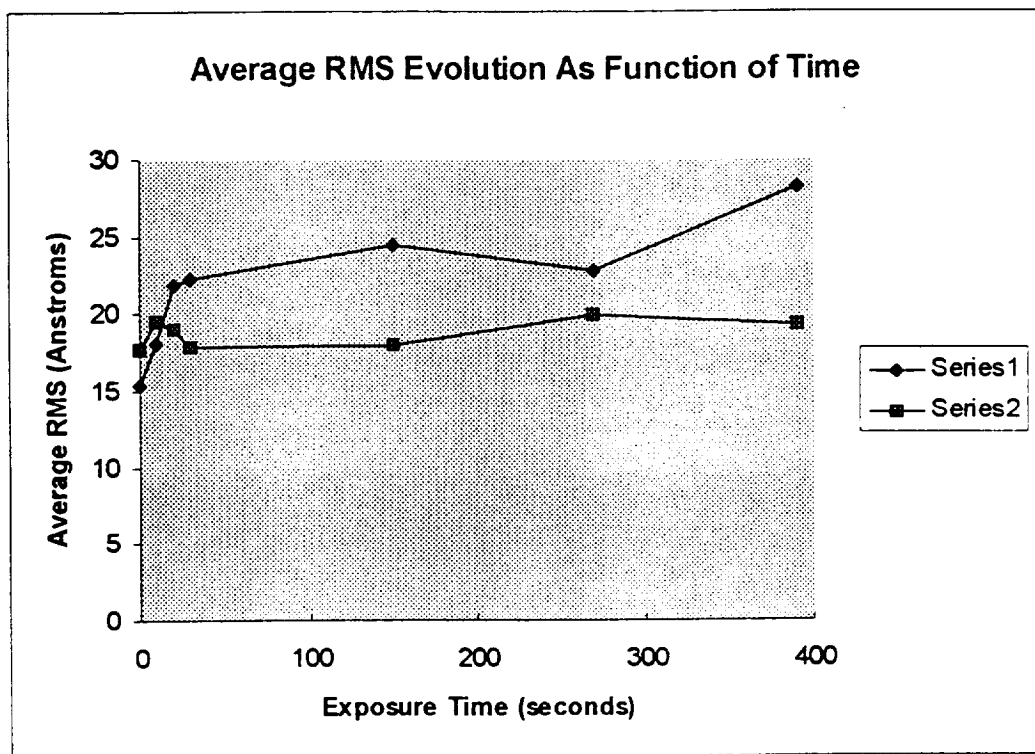**Figure 5.1**   Micrograph of diamond particles. |----------| 100 microns.

Average RMS Evolution As Function of Time

Figure 5.2   Average surface microroughness RMS evolution as a function of exposure time for diamond.

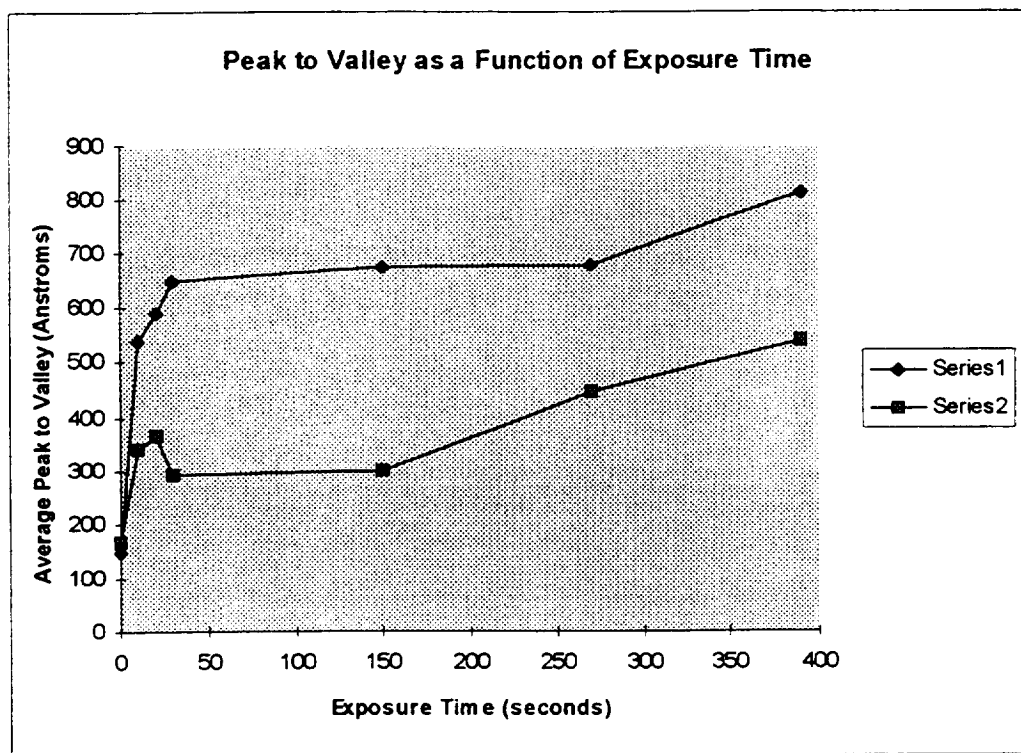**Peak to Valley as a Function of Exposure Time**

Figure 5.3   Average surface peak to valley as a function of exposure time for

diamond.

Not all the stickers can be attributed to the diamond embedding, some are the result of nickel rosettes crystallizing in the nickel[26] and dirt particles contaminating the plating bath during the plating process[27]. The stickers introduced by the plating process do not constitute a major concern until there populations exceed the number of stickers introduced by the polishing process.

The aluminum oxide compound showed none of the complications experienced with the diamond, with no apparent embedding of the polishing particles. The aluminum oxide is used with a pitch polish as opposed to the flocked polishing lap used with the diamond paste compound. The aluminum oxide was much more effective in reducing the surface microroughness RMS below the 15 angstrom barrier experienced by the diamond polish. The silica based colloidal was used following the aluminum oxide when the surface measured 13 angstroms RMS and reduced the surface further to 8 angstroms. The surface microroughness RMS was more resilient at holding its microroughness value, when exposed to the ion beam. The surface microroughness RMS in Figure 5.4 grew an average of two angstrom over the course of exposure to the ion beam. The evolution of the Peak to Valley ratio in Figure 5.5 shows a steady increase. The Peak to Valley ratio would be expected to increase slowly as the ion beam uncovers more and more defects in the plated nickel. The values presented above represent measurements at the center of the workpiece corresponding to the peak intensity of the ion beam. The beam center data is represented in Figures 5.2-5.5 by the Series 1 lines. The lower intensities and lower removal rates correspond to the edge of the beam and the edge of the workpiece. The edge data is represented by the Series 2 lines in Figures 5.2-5.5. Comparing the edge data

to the center data allows a reference for comparison where at the edge the material removed is a fraction of the amount removed in the center. The evolution of the RMS and Peak to Valley ratio can be seen to not rise as severely as the center data.
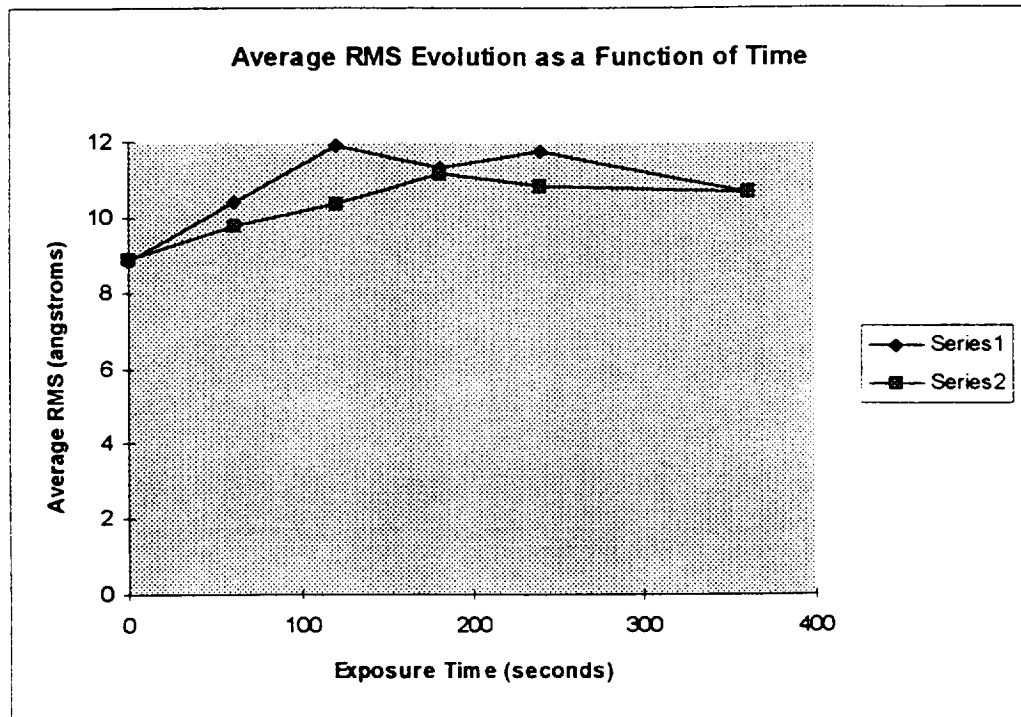
Average RMS Evolution as a Function of Time

Figure 5.5   Average surface microroughness RMS as a function of exposure

time for Al-O.

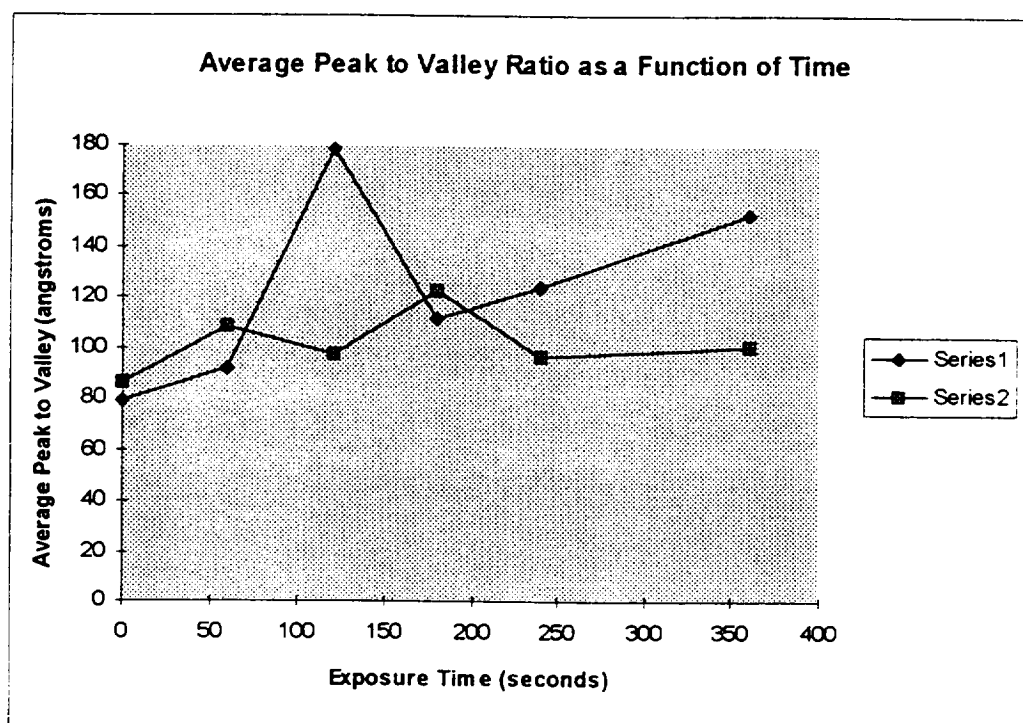**Average Peak to Valley Ratio as a Function of Time**

Figure 5.4   Average surface peak to valley ratio as a function of exposure time

for Al-O.

5.2. Results

Aluminum oxide followed by the silica based colloidal proved to be the superior polishing method. The ion beam final figuring process necessitates polishing the electroless nickel surface RMS down to these low microroughness regions with as little subsurface damage as possible. This will insure no or little increase in the surface RMS, assuming the material being figured is homogeneous. Diamond paste polish caused problems when it embedded in the nickel surface and should not be used to polish electroless nickel surfaces beyond 20 angstroms RMS.

These results can be applied to the current figuring task, of imparting a contour on a cylindrical mandrel plated with electroless nickel. An accurate account of the effects of ion figuring on the microroughness is essential in the deterministic figuring process.

If we know the material removal rate, as discussed in chapter 6, then the exposure time can correspond to a machining depth of the ion beam. The average RMS as a function of machining depth is shown in Figure 5.6.

An important factor not to be taken for granted is the homogeneity of the electroless nickel. Some plating is better than others, and it has been shown good plating can be achieved through vigilant care and individual attention to the desired plating performance. In one such case the ion beam transformed a RMS of 6 angstroms to 40 angstroms in the span of two minutes of exposure. The surface had a distinct cloudiness in the finish and consisted of primarily pits and holes. Using a scanning electron microscope the surface features could clearly be seen to be holes one micron in diameter as shown in Figure 5.7. The sample was previously stripped of nickel using a strong acid
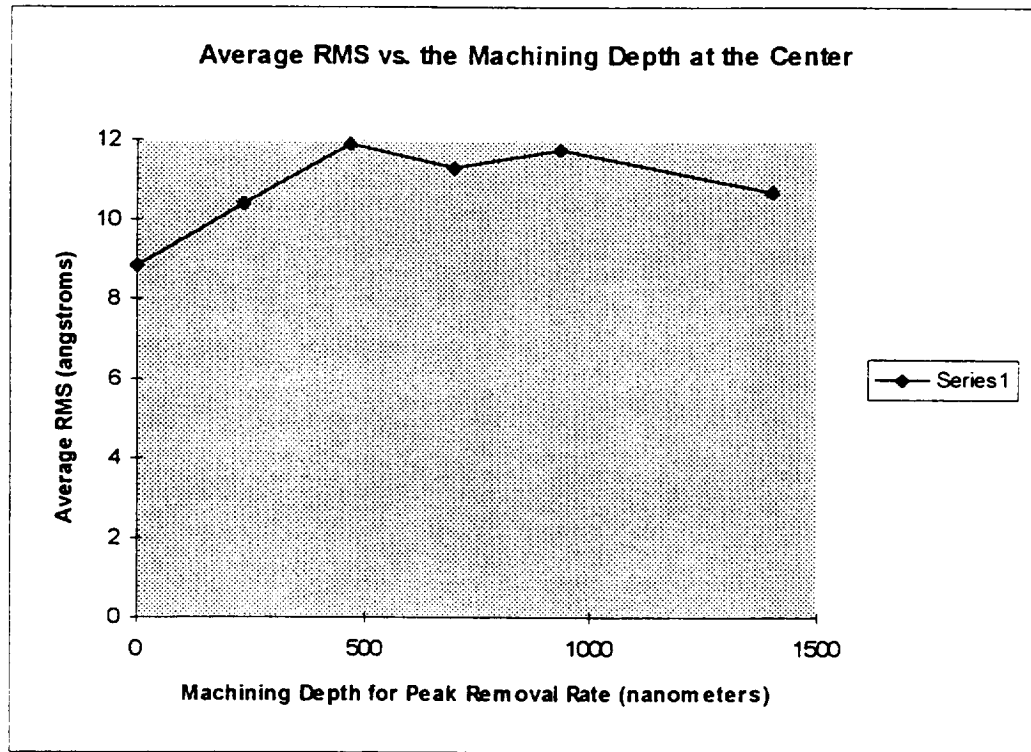
26

Average RMS vs. the Machining Depth at the Center

Figure 5.6   Average surface microroughness RMS vs. machining depth at the

center for Al-O.

E4046 2000   Clear area near edge
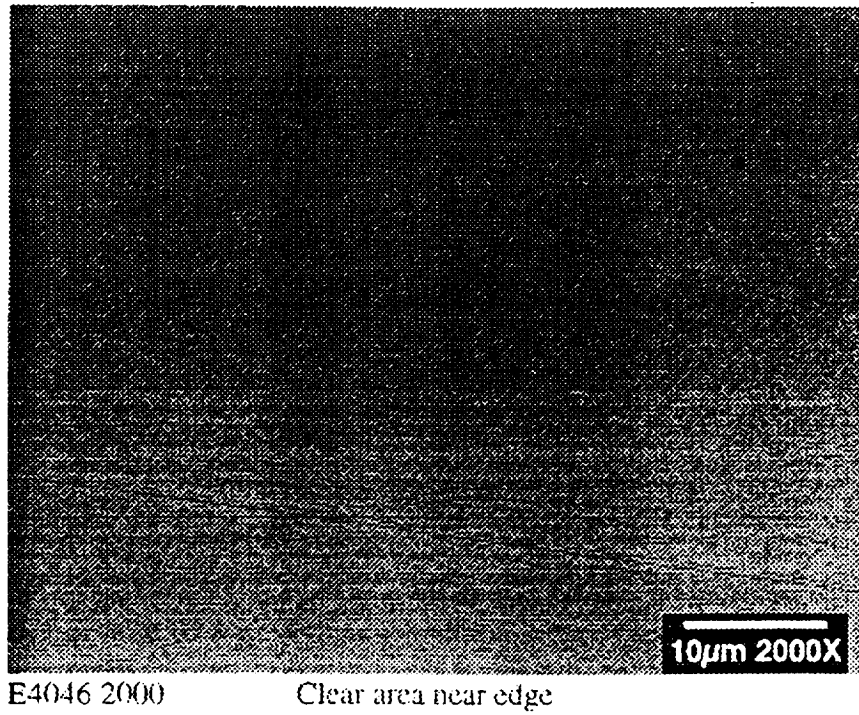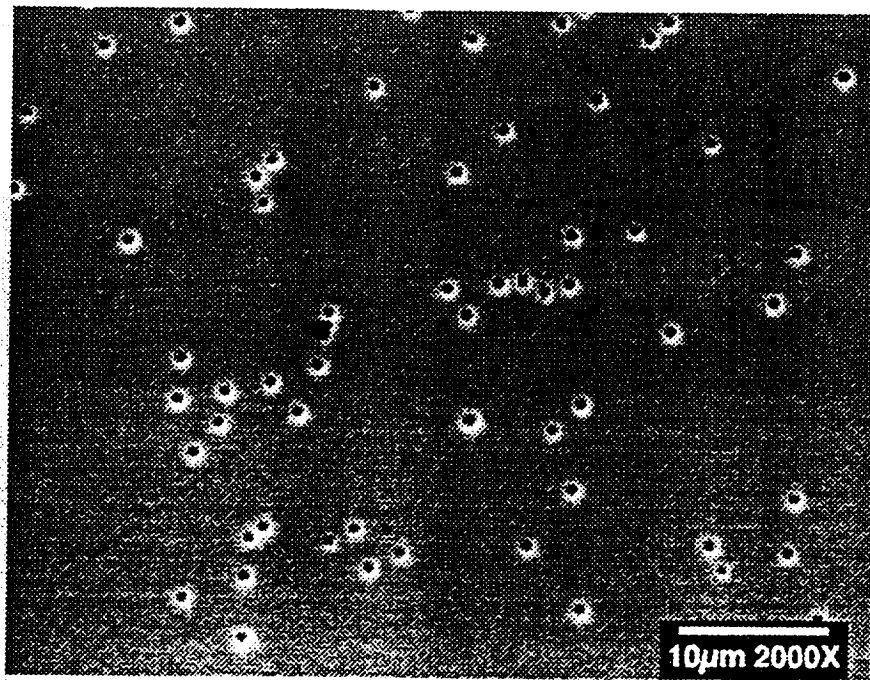
Figure 5.7   SEM image of surface at edge.

H0384 2000   Cloudy area in center

Figure 5.8   SEM image of surface at center.

and then replated with electroless nickel. It is suspected that the stripping process induced hydrogen into the aluminum substrate[27]. This would only be possible if the aluminum had defects and voids to accept the hydrogen. These defects are common in commercial aluminum bar stock, typically in the center of the bar due to rolling the high temperature aluminum into shape[27]. The sample after being stripped was then immediately plated with the electroless nickel. Without baking to cure the sample of any trapped gases, the hydrogen escaping can become trapped in the nickel plating forming voids. Exposure to the ion beam quickly reveals these voids, making the surface finish optically useless. The simple solution is to cure the sample by baking to insure against any trapped gases.

6. Beam Profile Experiments

It has been mentioned that the stability of the ion beam is vital to the deterministic nature of the ion beam figuring process. It is equally important to have an accurate measure and model of this stabile beam profile. The accuracy of the model of the ion beam profile will directly affect the performance and predictability of the ion figuring process. The beam function (ion beam profile) is deconvolved with the "hit" map to calculate the dwell function. The accurate representation of the ion beam function directly affects the accuracy of the dwell function. The ion figuring process could be compromised by inaccuracy in the beam function and cannot be expected to produce precision figuring results.

The ion beam profile has previously been approximated using a Gaussian distribution with great success[15]. B(x,y) is the beam function:

$$B(x,y) = \Gamma \exp\left[\frac{x^2 + y^2}{\omega^2}\right] \qquad (3)$$

Γ is the peak removal rate with units of nm/sec, ω is the beam width in millimeters and x and y are the Cartesian coordinates from the center of the ion beam as in Figure 6.1 (notice the symmetry in this approximation). The Gaussian distribution model is used in the PIMS with an emphasis on minimizing the width of the beam without compromising the beam peak removal rate. The width is a result of the acceleration voltage and the working distance. The removal rate likewise is related to the working distance, but is additionally affected by the beam current.
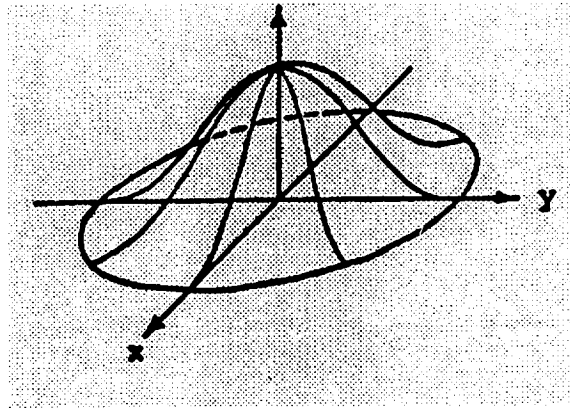
31

Figure 6.1   Gaussian Distribution model (where z-axis is the removal rate).

6.1. Beam Width

The beam width should be minimized to the smallest spot size in order to allow the ion beam to correct the smallest possible features. The beam width can be reduced by decreasing the acceleration voltage as discussed in chapter 4. Care must be taken not to decrease the acceleration voltage too much which allows the back flow of electrons from the neutralizing filament, thus shorting the ion source. The acceleration voltage plays a small role in the discharge current value, producing a discharge current of 0.88 amps requires that the acceleration voltage not fall below 200 volts. The beam width was calculated by taking the difference between Zernike polynomials of the initial and final surfaces of the sample after being exposed to the ion beam. The difference can then be approximated with a Gaussian distribution and then the width determined. The procedure is shown schematically in Figure 6.2. The ion beam is held stationary for determining the beam profile and held at a working distance of 2.5 inches from the workpiece. The width increases with the working distance as shown in Figure 6.3. The ideal working distance was found to be 1.5 inches. The distance was later increased to 2.5 inches because of residual traces of the neutralizing filament shadow were imprinting on the surface of the nickel. In Figure 6.4 the imprinting can be seen after 300 seconds of total exposure time to the ion beam. The best beam width for current purposes was 17 mm with an acceleration voltage of 200 volts and a working distance of 2.5 inches.
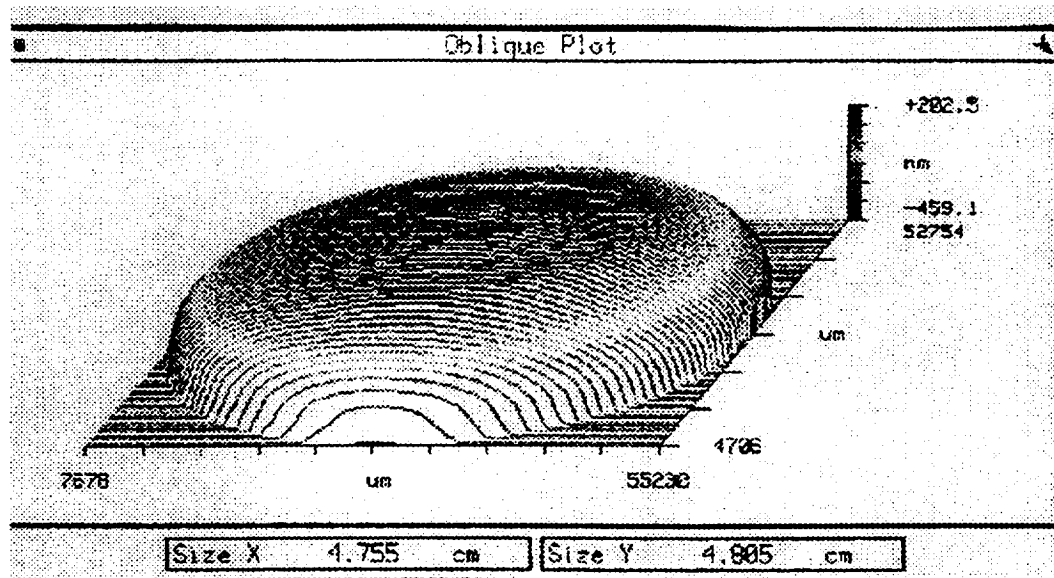
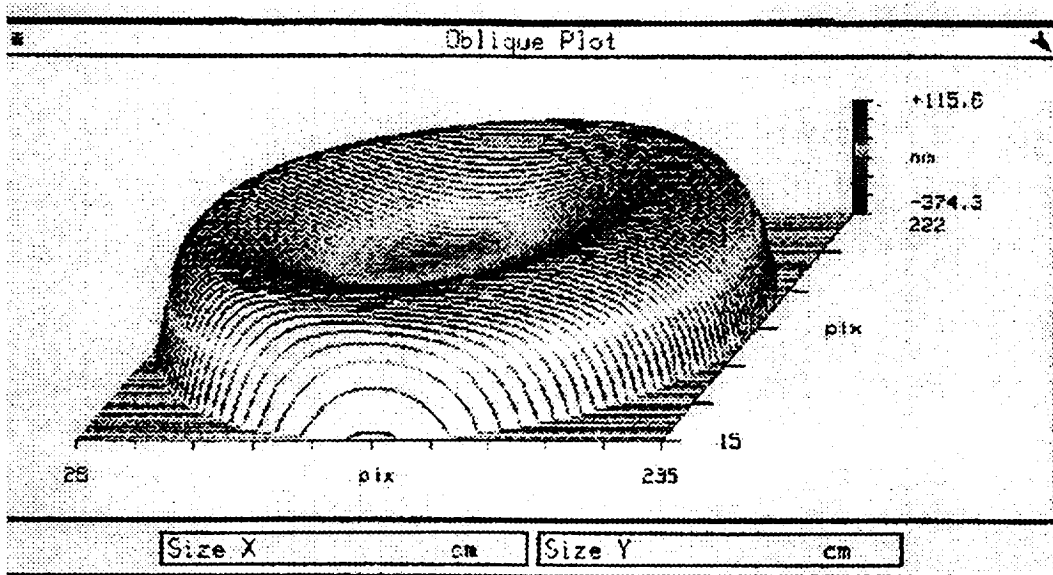Figure 6.2   Zernike subtraction method's initial surface.

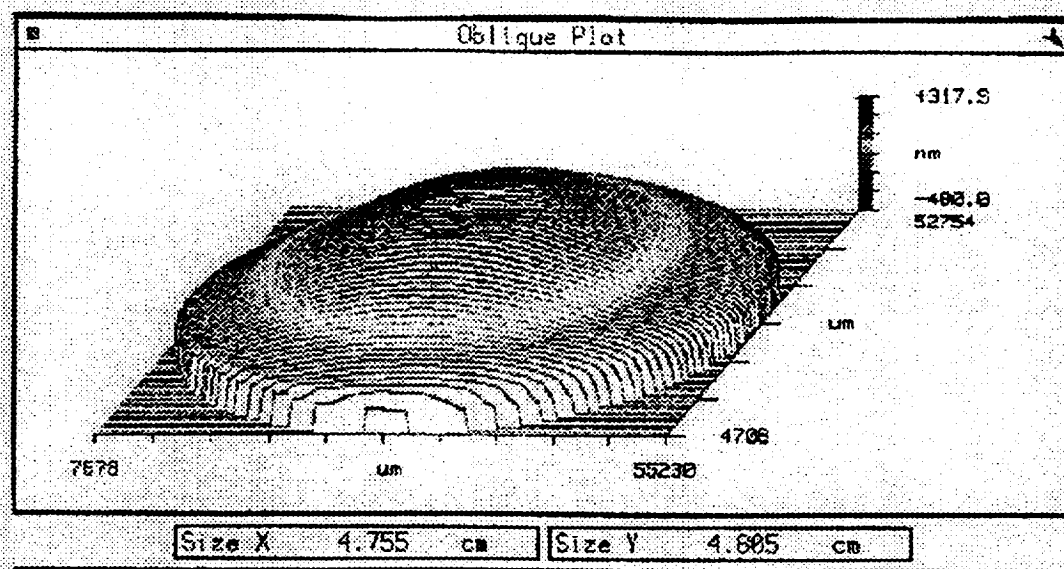Figure 6.3   Zernike subtraction method's final surface.

Figure 6.4　Zernike subtraction method's resulting Gaussian shape.
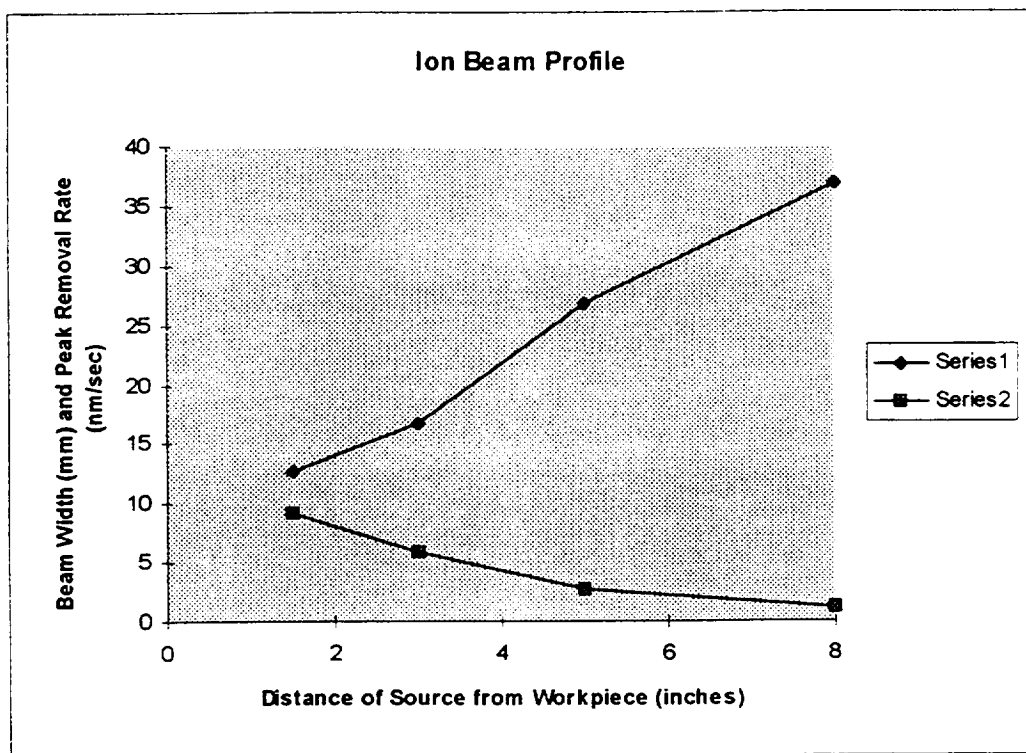
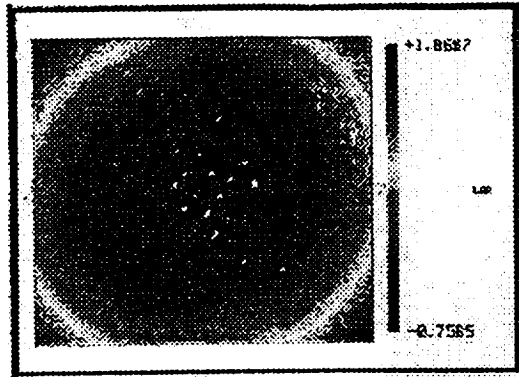Figure 6.5   Ion beam profile as a function of workpiece distance.

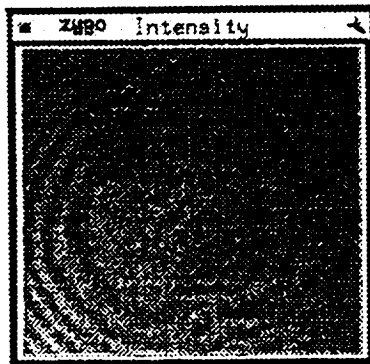Figure 6.6   Topographic map of the imprinted nickel surface.

Figure 6.7   Interferogram of the imprinted nickel surface.

6.2. Beam Peak Removal Rate

There are two procedures used in determining the peak removal rate, subtracting the Zernike polynomials as above and modeling with a Gaussian distribution, or masking half the workpiece to essentially have a zero to compare how much material is removed. The first method depends on the size of the part and if Zernike polynomials are readily available in the metrology system software.

The Zernike polynomial subtraction uses the same method as section 6.1 Beam Width, only the value of interest is the peak removal rate. This method makes two assumptions, first the workpiece is significantly larger than the beam width and therefore little material is removed at the workpiece edge. Then when the initial and post figured surfaces are subtracted, an accurate model of the material removed can be modeled with a Gaussian and the peak removal rate determined. If the workpiece is not significantly larger than the beam width, taking the difference between the initial and final surfaces to determine the material removed will be incorrect due to a significant amount of material being removed at the edge of the workpiece . There is not a technique to determine the piston in order to compensate for this effect without a mask. The second problem encountered with the Zernike subtraction is the error in the metrology and the Zernike modeling. The error can be compounded by the subtraction step and even doubled if the two surface errors add constructively.

An alternate determination of the peak removal rate can be achieved by masking half the workpiece and measuring the difference between the masked and unmasked regions. This can most easily be done using a trace profilometer to measure the linear

profile of the surface and then calculating the difference of the absolute height of the surface as the profile traverses the masked and unmasked regions. The peak removal rate measured by the LTP II using this procedure was 3.89 nanometers per second (+/- 1.00 nm/sec). The Zernike subtraction method (measured on a Zygo Mark IV interferometer) showed much more fluctuation, 10.25 nm/sec (+/- 3 nm/sec). The Zernike subtraction method was shown to have discrepancies in the methodology for the 2 inch diameter samples due to the sample size compared to the beam width. The LTP II, using the mask, provides a much more accurate measure for the removal rate. The removal rate is also affected by the beam current, which is proportional to the intensity exiting the ion source (and hence incident on the workpiece). An increase in beam current results in an increase in the removal rate. The beam current was maintained, for that reason, at 60 microamps throughout the experiments.

6.3. Results

The beam profile can be modeled with a Gaussian distribution with the values of the peak removal rate and the beam width inserted as shown:

$$B(x,y) = 3.89 \exp\left[\frac{x^2 + y^2}{17^2}\right] nm / sec. \tag{4}$$

Assuming the beam profile is an accurate model, it can be used as the beam function to determine the dwell function in the deconvolution. The importance of metrology arises again in determining the beam function, as is the case with the "hit" map calculation. The limits in the deterministic behavior of the ion beam figuring process is in the measurements and calculations of the surface being figured.

7. Cylindrical Mandrel Metrology

The mapping of a cylindrical optic is an interesting and challenging problem which NASA's Marshall Space Flight Center (MSFC) is posed to solve. MSFC produces grazing incident X-ray optics from nickel plated cylindrical mandrels in its replicated optics laboratories. Currently the metrology technique used to map the contour of the cylindrical optic is a Long Trace Profilometer, LTP II, with a working distance of one meter. The present problem with this method is that there is not a way to compare the mandrel contour to the desired ideal contour. Use of the profilometer further introduces the assumption of axial symmetry of the mandrel, because the profilometer is only able to scan radially. An alternate method is to interferometrically map the contour using an experimental procedure explored by Joseph Geary[21]. This method promises to be much more informative and does not assume axial symmetry.

7.1. Long Trace Profilometer Measurements on X-ray Optic Mandrels

The Long Trace Profilometer (LTP II) is an instrument employed at MSFC developed by Continental Optical Corporation for mapping contour profiles up to a meter in length. The LTP II has the potential to measure RMS with an accuracy capability in the height profile of less than 3 nm over the full 1 meter range, excluding error introduced by thermal drift[28]. The LTP II measures the mandrel by tracing the test probe beam down the axis of the mandrel surface. The test and reference probe beams generate a path difference which is converted to absolute height data. The surface contour can then be determined and corrected for errors inherent in the optical system. The measured contour

41

can be compared to the ideal contour to generate a "hit" map. The major drawback is the LTP can only measure axially and provides no information on the angular deviations of the mandrel and hence axial symmetry must be assumed to proceed.

7.2. Interferometry Measurements on X-ray Optic Mandrels

The search of a more realistic model of the surface contour leads to interferometry analysis. Previous research has been conducted by Joseph Geary [21] using interferometry to measure the contour of grazing incident optics. The contour of the cylindrical mandrel is very critical in the replication of optics that will be redirecting high energy X-rays sensitive to the slightest aberration. Therefore it becomes quite necessary to have the ability to measure the surface contour as accurately as possible.

The first step is to characterize the cylindrical optic for any aberrations to allow for the correction of the cylindrical wavefront impinging on the mandrel. This is accomplished by comparison of the cylindrical optic to a cylindrical fiber optic as demonstrated by Geary[22]. The second step would be to perform the actual measurement on the mandrel and obtain an interferogram. Subtracting the ideal interferogram from the mandrels interferogram will produce the surface's actual contour. The actual contour is then improved upon by subtracting out the aberrations measured in the cylindrical lens. The result should be the actual surface contour of the mandrel region in question.

7.3. Discussion

The LTP II promises a quick result to the contour mapping problem at the cost of reducing the information by one dimension. If the mandrels are indeed axially symmetric this method would be more than adequate. If more information is required and axial symmetry cannot be taken for granted, then interferometry analysis would be an excellent approach.

8. Discussion

The objective of this research was to be able to impart a contour on a cylindrical mandrel made of aluminum with a polished electroless nickel surface. The beam function, established from the above research, provides information on removal rate and its effect on the electroless nickel surface. This beam function is consequently a removal rate profile at perpendicular incidence. It must be determined whether this flat approximation is sufficient for cylindrical targets or if the beam function must be modified to account for non-perpendicular incidences expected when figuring a cylinder. Presently, there is a lack of information in measuring cylindrical optics. This step will help determine the beam function for cylindrical optics and map the contour to determine a "hit" map. Finally, a control system will be necessary to automate the process and assure precision.

The ion beam removal rate has been shown to increase at incidences greater than 15 degrees[18]. It must be determined if the beam width will surpass this angular incidence when impinging on the mandrel surface, and if it does, how will this affect the beam removal rate profile. The angular removal rates can be determined just as the normal incident removal rates were, using a mask as in chapter 6. The beam function can then be adjusted accordingly to conform to the cylindrical mandrel surface and radius of curvature.

A critical point to be investigated in the future is the comparison between two different mandrel contours, and between the measured and ideal contours. Two mapping techniques are discussed in Chapter 7 which show promise in providing an informative map of the cylindrical contour. This step is important in developing a method to measure

and provide a "hit" map or removal map. This information can then be taken with the beam function and deconvolved to determine the dwell function. The dwell function will fix the velocities at which the ion beam will be scanned across the workpiece. These calculations are more involved than they appear and require a possible Fourier transform or a series-derivative solution[14,16] for the deconvolution. The series-derivative solution is very successful in reducing the noise sensitivity and converged rapidly to near the ideal final figure[16]. The two limiting agents in this step will be the metrology and the means to which we represent that metrology through the deconvolution.

The control system must be able to manipulate the mandrel to a precision prescribed by the resolution of the beam function and the "hit" map. The specific velocities must be generated in order to resolve with the dwell function and the correct figuring performance. There are a number of different mandrels and one system cannot be expected to final figure for all of them. The 9 inch cylindrical mandrels can currently be housed in the 1 meter PIMS. The PIMS should be an adequate system to show that ion beam figuring can impart a contour on a mandrel.

9. Conclusion

Ion beam figuring shows great potential in the final figuring of optics and can fully be expected to be able to correct surface errors on cylindrical optics as well. The purpose of the experiments here was to demonstrate ion beam figuring effects on electroless nickel. It was important to establish that ion beam figuring did not induce any adverse effects to the nickel surface. This had been a problem with earlier ion accelerators causing radiation damage to the optical surface, addressed in chapter 2[6]. The results in chapter 5 show no significant degradation in the surface finish when polishing with an aluminum oxide compound followed by a silica based colloidal. The effects of subsurface damage are given great importance in the outcome of a quality optic. When using ion beam figuring for the final figuring it is critical to have a stress free surface and subsurface devoid of defects or damage. The ion beam has consistently been shown to be an excellent indicator of the quality of the subsurface. Polishing is not the only cause for failure in the ion beam final figuring process, the material composition is equally important. For ideal removal of material the material being figured has to be as close to homogeneous as possible. Only by careful consideration of both limiting factors can the ion beam final figuring process achieve its greatest potential.

The secondary goal was to construct a model for representing the ion beam material removal rate. Representing the ion beam removal rate is only an approximation and has a number of limiting factors in its accuracy. The use of a Gaussian distribution provides nice symmetry and compact representation, but also leaves out possible higher order approximations. The resolution of the metrology apparatus limits the modeling of

the beam function as well. As the surface error corrections demand more precision in the final figuring, the model representing the beam function must equally be precise. The precision to which the beam function can be represented is not only determined by the model but also by the measurements producing that model.

The method for determining the beam function can be applied to any material destined to be ion beam figured. The model representing the beam function on electroless nickel is adequate for the final figuring process and promises to provide good results.

REFERENCES

[1]   Meinel, A., S. Bashkin and D. Loomis. 1965. "Controlled Figuring of Optical Surfaces by Energetic Ionic Beams," *Applied Optics 4*, pp. 1675.

[2]   Schroeder, J., H. Dieselman and J. Douglass. 1971. "Technical Feasibility of Figuring Optical Surfaces by Ion Polishing," *Applied Optics 10*, pp. 295.

[3]   Bayly, A. and P. Townsend. 1972. "Glass machining by ion sputtering," *Journal of Physics D: Applied Physics 5*, pp. L103.

[4]   Schroeder, S., S. Bashkin and J. Nester. 1966. "Ionic Polishing of Optical Surfaces," *Applied Optics 5*, pp. 1013.

[5]   Yasuda, H. 1973. "Figuration of Wedge-Shaped and Parabolic Surfaces by Ion Etching," *Japanese Journal of Applied Physics*, 12, pp. 1139.

[6]   Wilson, S. R. 1987. "Ion Beam Figuring of Optical Surfaces," MS Thesis: The University of New Mexico, Albuquerque, New Mexico.

[7]   House, R., J. Bettis and A. Guenther. 1987. "Efficacy of Ion Polishing Optical Surfaces," *Applied Optics 6*, pp. 1486.

[8]   Schroeder, J., H. Diesel and J. Douglass. 1971. "Technical Feasibility of Figuring Optical Surfaces by Ion Polishing," *Applied Optics 10*, pp. 295.

[9]   Kaufman, H. 1984. *Fundamentals of Ion Source Operation*. Commonwealth Scientific Corporation, Alexandria, VA.

[10]   Allen, L. N. and R. E. Keim. 1989. "An Ion Figuring System for Large Optic Fabrication," SPIE, Vol. 1168, pp. 33-50.

[11]   Allen, L. N., R. E. Keim and T. S. Lewis. 1991. "Surface Error Correction of a Keck 10m Telescope Primary Mirror Segment by Ion Figuring," Eastman Kodak Company, Federal Systems Division, Rochester, NY.

[12]   Allen, L. N., J. J. Hannon and R. W. Wambach. 1991. "Final Surface error correction of an off-axis aspheric petal by ion figuring," Eastman Kodak Company, Federal Systems Division, Rochester, NY.

[13]   Carnal, C. L., C. M. Egert and K. W. Hylton. 1992. "Advanced Matrix-Based Algorithm for Ion Beam Milling of Optical Components," *Society of Photo-Optical Instrumentation Engineers*, San Diego, CA.

[14]   Drueding, T. W. 1995. "Precision Ion Figuring System for Optical Components,"
        Ph.D. Dissertation: Boston College, College of Engineering, Boston, Mass.

[15]   Drueding, T. W., S. C. Fawcett, S. R. Wilson, T. G. Bifano. December 1995. "Ion
        beam   figuring of small optical components," *Optical Engineering*, Vol. 34, No. 12,
        pp. 3565.

[16]   Drueding, T. W., T. G. Bifano, S. C. Fawcett. 1995. "Contouring algorithm for ion
        figuring," *Precision Engineering*, Vol. 17, pp. 10-21.

[17]   Ghigo, M. O. Citterio, P. Conconi, R. Loi, F. Mazzoleni. September 1995.
        "Perspectives of ion-beam polishing of mandrels for X-ray replication optics," *SPIE*,
        Vol. 2515, pp. 55-63.

[18]   Carter, G., M. Nobes, I. Katardjiev. March-April 1993. "The theory of Ion Beam
        Polishing and Machining," *Vacuum*, Vol. 44, pp. 303-309.

[19]   Carter, G., M. Nobes. 1991. "The principles of a New Method of Determining Ion
        Beam Profile Density of Distribution," *Vacuum*, Vol. 42, No. 17, pp. 1125-1128.

[20]   Ion Tech, Inc. November 1991. "3 cm Ion Source Manual," Fort Collins, CO.

[21]   Geary, J. M., R. Maeda. December 1987. "Interferometry on grazing incidence optics,"
        Optical Engineering, Vol. 26, No. 12, pp. 1225.

[22]   Geary, J. M. March 1989. "Interferometry on Wolter X-ray optics: a possible
        approach," *Optical Engineering*, Vol. 28, No. 3, pp. 217.

[23]   Ion Tech, Inc. July 1996. Instruction Manual MPS-3000 Power Supply, Fort Collins,
        CO.

[24]   Ion Tech, Inc. April 1989. Instruction Manual GFC-1000 Gas Flow Controller, Fort
        Collins, CO.

[25]   Drueding, T. W., S. C. Fawcett, T. G. Bifano. March 1994. *"Neutral ion figuring of
        chemical vapor deposited SiC,"* Optical Engineering, Vol. 33, No. 3, pp. 967.

[26]   Mayer, A., R. D. Bramlett, R. D. Day, C. J. Evans, R. S. Polvani. *"Electrodeposited
        coatings for diamond turning applications,"* Los Alamos National Laboratory and
        National Institute of Standards and Technology.

[27]   Engelhaupt, D. 1997. Correspondence and insight into electroless nickel plating, UAH.

[28]   Continental Optical Corporation. January 1995. LTP II Manual of Operation,
        Hauppauge, NY.